

Probing Fundamental Physics with the Cosmic Microwave Background: Present Status and Future Prospects

Martin BUCHER, Laboratoire Astroparticles & Cosmologie,
Université Paris 7 (Denis-Diderot)/CNRS
Paris, France

and

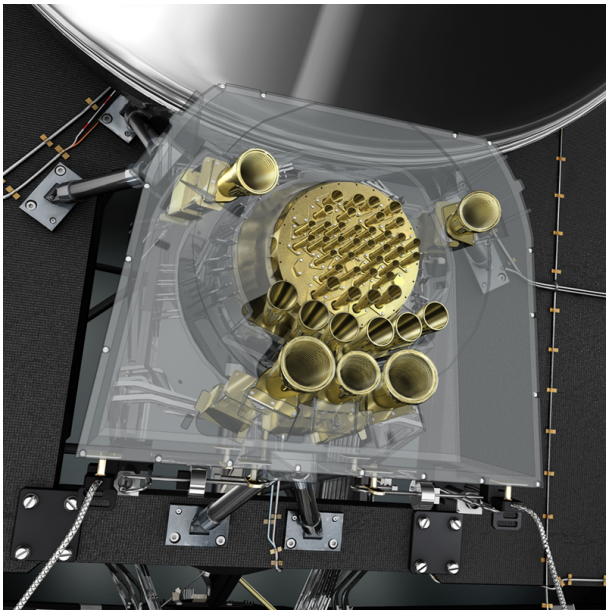
University of KwaZulu-Natal, Durban, South Africa

19 February 2018, Tata Institute of Fundamental Research,
Mumbai, India

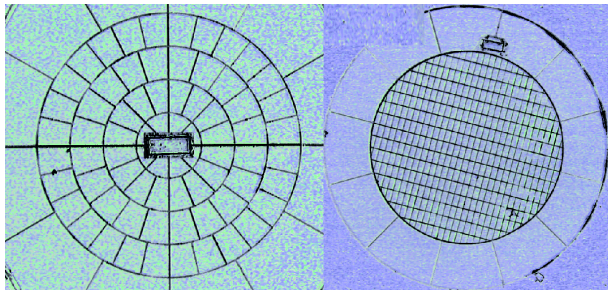
The *Planck* mission



PLANCK Focal Plane



The Workhorse of Planck : Spiderweb and Polarization Sensitive Bolometers

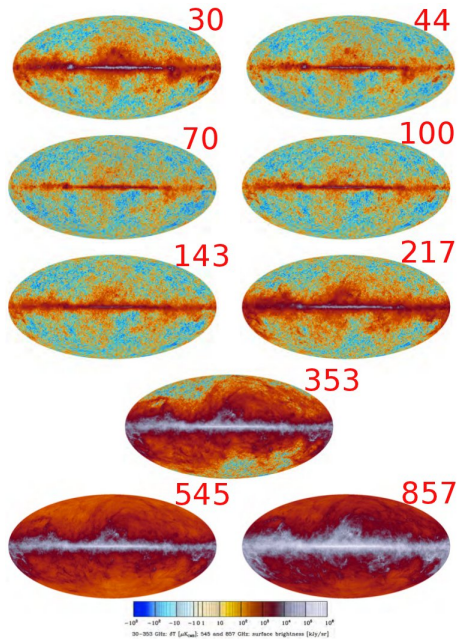


Made by JPL, Caltech
Cooled to $\approx 100\text{ mK}$

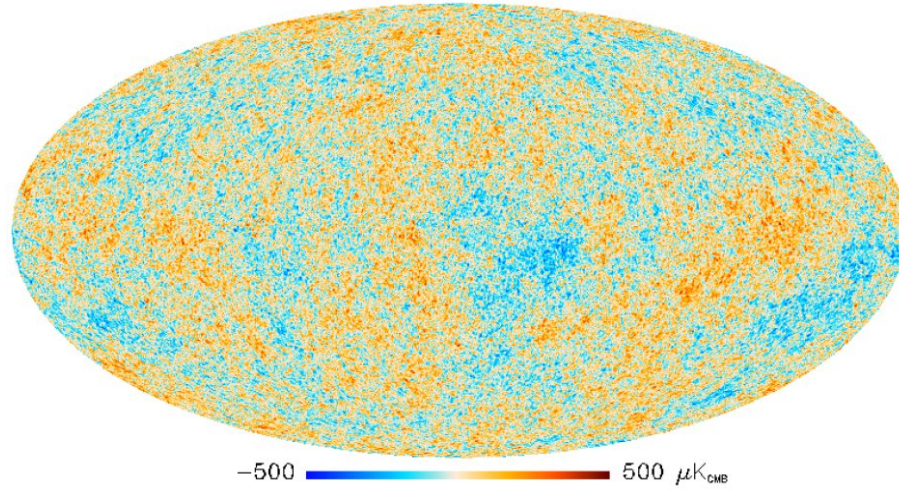
Planck Capabilities

Table 2. *Planck* performance parameters determined from flight data.

CHANNEL	$N_{\text{detectors}}^{\text{a}}$	$\nu_{\text{center}}^{\text{b}}$ [GHz]	SCANNING BEAM ^c		NOISE ^d SENSITIVITY	
			FWHM [arcmin]	Ellipticity	[$\mu\text{K}_{\text{RJ}} \text{s}^{1/2}$]	[$\mu\text{K}_{\text{CMB}} \text{s}^{1/2}$]
30 GHz	4	28.4	33.16	1.37	145.4	148.5
44 GHz	6	44.1	28.09	1.25	164.8	173.2
70 GHz	12	70.4	13.08	1.27	133.9	151.9
100 GHz	8	100	9.59	1.21	31.52	41.3
143 GHz	11	143	7.18	1.04	10.38	17.4
217 GHz	12	217	4.87	1.22	7.45	23.8
353 GHz	12	353	4.7	1.2	5.52	78.8
545 GHz	3	545	4.73	1.18	2.66	0.0259 ^d
857 GHz	4	857	4.51	1.38	1.33	0.0259 ^d



Planck ILC map



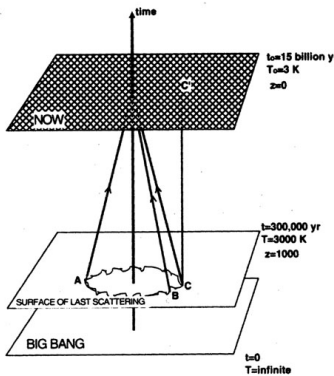
Theory – origin of the CMB anisotropy

Sachs-Wolfe formula

$$\frac{\delta T}{T}(\hat{n}) = \left[\frac{1}{4} \delta_\gamma + \mathbf{v}_\gamma \cdot \mathbf{n} + \Phi_i \right]_i^f + 2 \int_i^f d\eta \frac{\partial \Phi'}{\partial \eta} (\eta, \hat{n}(\eta_0 - \eta))$$

Φ \equiv Newtonian gravitational potential (dimensionless)

δ_γ and \mathbf{v}_γ describe the fractional density contrast and peculiar 3-velocity of the photon component.



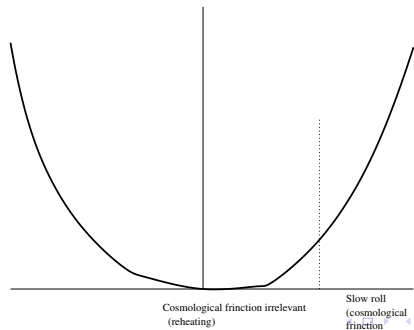
This treatment is somewhat naive because it assumes that the surface of last scatter is infinitely thin.

In reality the surface of last scatter has a width the smears the anisotropies on small scales.

Single-Field Inflation

In the beginning there was a scalar field that dominated the universe. Everything came from this scalar field and there was nothing without the scalar field. The quantum fluctuations of this field (that is, those of the vacuum) generated small fluctuations that advanced or retarded the instant of re-heating. These were the seeds of the large-scale structure.

$$\ddot{\phi} + 3H\dot{\phi} = -V_{,\phi}$$



Perturbations generated during inflation

$$\hbar = c = 1, M_{pl}^{-2}$$

$$\delta\phi \approx H \quad \frac{\delta\rho}{\rho} \approx H \cdot \delta t, \quad \delta t \approx \frac{\delta\phi}{\dot{\phi}}$$

$$H\dot{\phi} \approx V_{,\phi}, \quad \dot{\phi} \approx V_{,\phi}/H, \quad H^2 \approx \frac{1}{M_{pl}^2} V, \quad \frac{\delta\rho}{\rho} \approx \frac{V^{3/2}[\phi(k)]}{M_{pl}^3 V_{,\phi}}$$

Scalar perturbations :

$$\mathcal{P}_S^{1/2}(k) \approx O(1) \cdot \frac{V^{3/2}[\phi(k)]}{M_{pl}^3 V_{,\phi}[\phi(k)]}.$$

Tensor perturbations :

$$\mathcal{P}_T^{1/2}(k) \approx O(1) \cdot \frac{H}{M_{pl}} \approx O(1) \cdot \frac{V^{1/2}}{M_{pl}^2}$$

$\phi(k) \equiv$ value of ϕ at horizon crossing of the mode k

Reconstruction of the inflationary potential : the tensors measure the height of the potential, the scalars the slope.

Planck temperature (TT) power spectrum+residuals

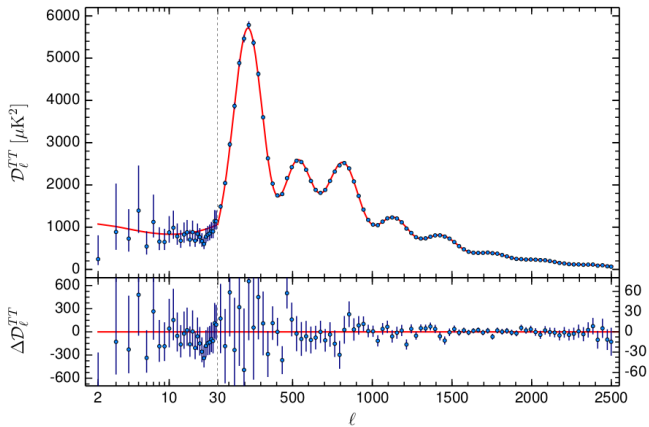
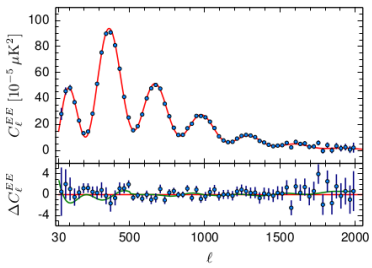
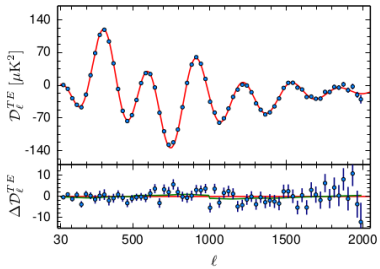


Fig. 1. The *Planck* 2015 temperature power spectrum. At multipoles $\ell \geq 30$ we show the maximum likelihood frequency averaged temperature spectrum computed from the *Plik* cross-half-mission likelihood with foreground and other nuisance parameters determined from the MCMC analysis of the base ΛCDM cosmology. In the multipole range $2 \leq \ell \leq 29$, we plot the power spectrum estimates from the *Commander* component-separation algorithm computed over 94% of the sky. The best-fit base ΛCDM theoretical spectrum fitted to the *Planck* TT+lowP likelihood is plotted in the upper panel. Residuals with respect to this model are shown in the lower panel. The error bars show $\pm 1\sigma$ uncertainties.

Planck polarization (TE+EE) power spectra+residuals



The six-parameter concordance model

[1] Parameter	[2] 2013N(DS)	[3] 2013F(DS)	[4] 2013F(CY)	[5] 2015F(CHM)	[6] 2015F(CHM) (Plik)	$([2] - [6])/\sigma_{[6]}$	$([5] - [6])/\sigma_{[5]}$
$100\theta_{\text{MC}}$	1.04131 ± 0.00063	1.04126 ± 0.00047	1.04121 ± 0.00048	1.04094 ± 0.00048	1.04086 ± 0.00048	0.71	0.17
$\Omega_b h^2$	0.02205 ± 0.00028	0.02234 ± 0.00023	0.02230 ± 0.00023	0.02225 ± 0.00023	0.02222 ± 0.00023	-0.61	0.13
$\Omega_c h^2$	0.1199 ± 0.0027	0.1189 ± 0.0022	0.1188 ± 0.0022	0.1194 ± 0.0022	0.1199 ± 0.0022	0.00	-0.23
H_0	67.3 ± 1.2	67.8 ± 1.0	67.8 ± 1.0	67.48 ± 0.98	67.26 ± 0.98	0.03	0.22
n_s	0.9603 ± 0.0073	0.9665 ± 0.0062	0.9655 ± 0.0062	0.9682 ± 0.0062	0.9652 ± 0.0062	-0.67	0.48
Ω_m	0.315 ± 0.017	0.308 ± 0.013	0.308 ± 0.013	0.313 ± 0.013	0.316 ± 0.014	-0.06	-0.23
σ_8	0.829 ± 0.012	0.831 ± 0.011	0.828 ± 0.012	0.829 ± 0.015	0.830 ± 0.015	-0.08	-0.07
τ	0.089 ± 0.013	0.096 ± 0.013	0.094 ± 0.013	0.079 ± 0.019	0.078 ± 0.019	0.85	0.05
$10^9 A_s e^{-2r}$	1.836 ± 0.013	1.833 ± 0.011	1.831 ± 0.011	1.875 ± 0.014	1.881 ± 0.014	-3.46	-0.42

Parameterization of primordial power spectrum used here :

$$P(k) = A_S (k/k_p)^{ns}$$

Consistency of P with T ?

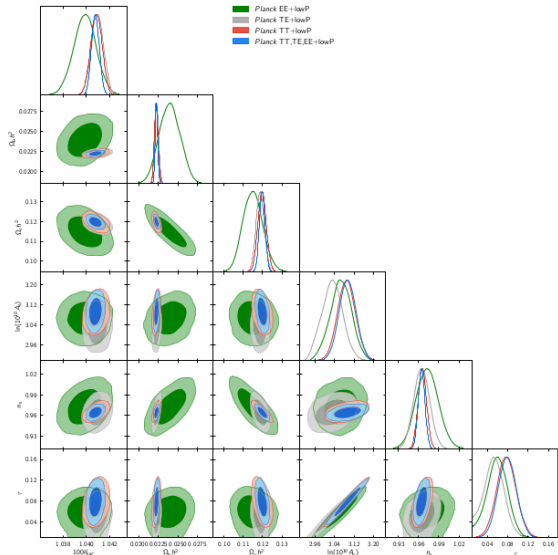


Fig. 6. Comparison of the base Λ CDM model parameter constraints from Planck temperature and polarization data.

Constraints on inflationary models

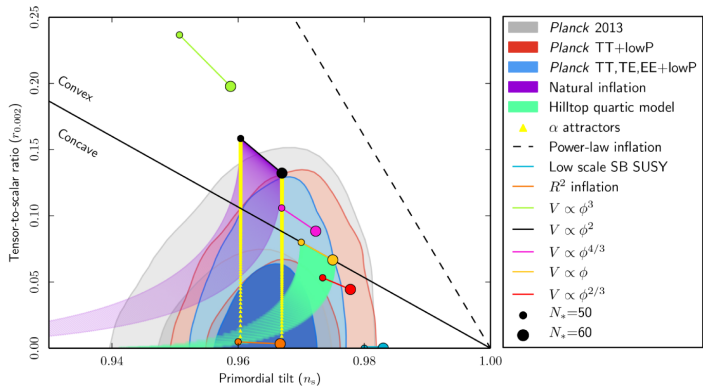


Fig. 12. Marginalized joint 68 % and 95 % CL regions for n_s and $r_{0.002}$ from *Planck* in combination with other data sets, compared to the theoretical predictions of selected inflationary models.

Planck Gravitational lensing spectrum

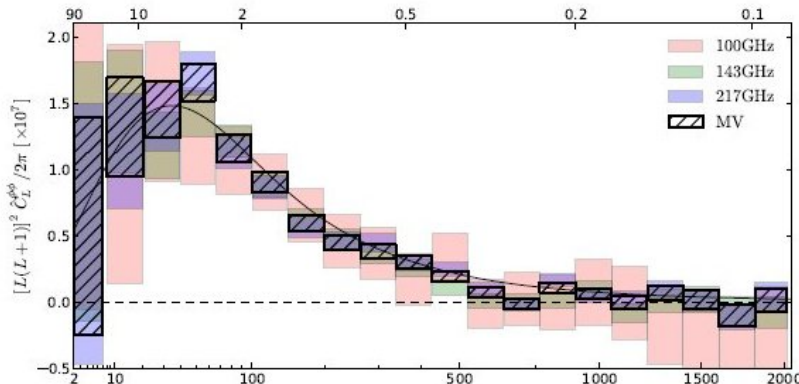


Fig. 18. Fiducial lensing power spectrum estimates based on the 100, 143, and 217 GHz frequency reconstructions, as well as the minimum-variance reconstruction that forms the basis for the *Planck* lensing likelihood.

Planck 2013 Results. XXIV. Constraints on primordial non-Gaussianity

Planck Collaboration : P. A. R. Ade, N. Aghanim, C. Armitage-Caplan, M. Arnaud, M. Ashdown, F. Atrio-Barandela, J. Aumont, C. Baccigalupi, A. J. Banday, R. B. Barreiro, J. G. Bartlett, N. Bartolo, E. Battaner, K. Benabed, A. Benoît, A. Benoit-Lévy, J.-P. Bernard, M. Bersanelli, P. Bielewicz, J. Bobin, J. J. Bock, A. Bonaldi, L. Bonavera, J. R. Bond, J. Borrill, F. R. Bouchet, M. Bridges, M. Bucher, C. Burigana, R. C. Butler, J.-F. Cardoso, A. Catalano, A. Challinor, A. Chamballu, L.-Y. Chiang, H. C. Chiang, P. R. Christensen, S. Church, D. L. Clements, S. Colombi, L. P. L. Colombo, F. Couchot, A. Coulais, B. P. Crill, A. Curto, F. Cuttaia, R. D. Davies, R. J. Davis, P. de Bernardis, A. de Rosa, G. de Zotti, J. Delabrouille, J.-M. Delouis, F.-X. Désert, J. M. Diego, H. Dole, S. Donzelli, et al. (175 additional authors not shown) (Submitted on 20 Mar 2013)

The Planck nominal mission cosmic microwave background (CMB) maps yield unprecedented constraints on primordial non-Gaussianity (NG). Using three optimal bispectrum estimators, separable template-fitting (KSW), binned, and modal, we obtain consistent values for the primordial local, equilateral, and orthogonal bispectrum amplitudes, quoting as our final result $f_{NL}^{local} = 2.7 \pm 5.8$,

$f_{NL}^{equil} = -42 \pm 75$, and $f_{NL}^{ortho} = -25 \pm 39$ (68% CL statistical); and we find the integrated Sachs-Wolfe lensing bispectrum expected in the Λ CDM scenario. The results are based on comprehensive cross-validation of these estimators on Gaussian and non-Gaussian simulations, are stable across component separation techniques, pass an extensive suite of tests, and are confirmed by skew- C_I , wavelet bispectrum and Minkowski functional estimators. Beyond estimates of individual shape amplitudes, we present model-independent, three-dimensional reconstructions of the Planck CMB bispectrum and thus derive constraints on early-Universe scenarios that generate primordial NG, including general single-field models of inflation, excited initial states (non-Bunch-Davies vacua), and directionally-dependent vector models. We provide an initial survey of scale-dependent feature and resonance models. These results bound both general single-field and multi-field model parameter ranges, such as the speed of sound, $c_s \geq 0.02$ (95%CL), in an effective field theory parametrization, and the curvaton decay fraction $r_D \geq 0.15$ (95%CL). The Planck data put severe pressure on ekpyrotic/cyclic scenarios. The amplitude of the four-point function in the local model $\tau_{NL} < 2800$ (95%CL). Taken together, these constraints represent the highest precision tests to date of physical mechanisms for the origin of cosmic structure.

NEW RESULTS ON THE REIONIZATION OPTICAL DEPTH

Planck 2016. Planck constraints on reionization history (astro-ph/1605.03507)

Planck 2016. Reduction of large-scale systematic effects in HFI polarization maps and estimation of the reionization optical depth (astro-ph/1605.02985)

Reionization optical depth (τ) / scalar perturbation amplitude (A_S) degeneracy

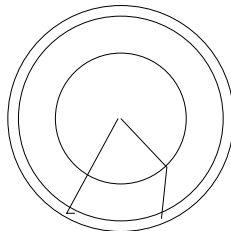
- ▶ The overall amplitude of the high- ℓ CMB anisotropies depends on the combination

$$A_S \exp[-\tau].$$

Only effects at very low ℓ break this degeneracy.

- ▶ The E-mode polarization is the cleanest way to break this degeneracy. The height of the reionization bump is proportional to τ (assuming $\tau \lesssim 1$.)
- ▶ Some other independent determination of A_S can likewise break this degeneracy (e.g., CMB lensing).

The Reionization Bump



It turns out that

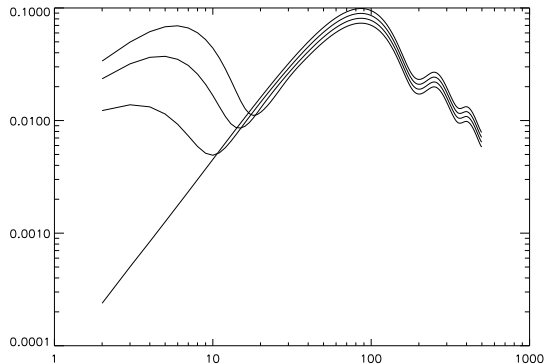
$$P \propto (1 - \tau) d_{lastscatter}^2 \frac{\partial^2 T}{\partial x^2}$$

is small compared to

$$P \propto \tau d_{reion}^2 \frac{\partial^2 T}{\partial x^2}$$

even when τ is small.

CMB polarization and the Reionization Bump



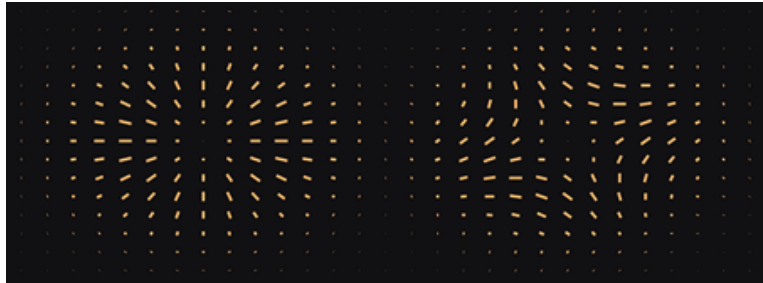
$\tau = 0.0, 0.5, 0.10, 0.15$ (bottom \rightarrow top)

CMB measurements of the reionization optical depth

- ▶ WMAP first year (based on TE, because EE was not available)
 $\tau = 0.17 \pm 0.04$
- ▶ WMAP third year (mainly based on low- ℓ EE) $\tau = 0.09 \pm 0.03$
- ▶ WMAP nine-year (last word from WMAP) $\tau = 0.089 \pm 0.014$
- ▶ WMAP cleaned with Planck 353 GHz dust map $\tau = 0.075 \pm 0.013$
- ▶ Planck 2013 – (not really an independent measurement, because Planck low- ℓ polarization not available)
 $\tau = 0.089 \pm 0.032$ Planck TT+lensing
- ▶ Planck 2015 release
 - $\tau = 0.078 \pm 0.019$ LFI 70 GHz Polar only
 - $\tau = 0.066 \pm 0.016$ (with lensing added)
 - $\tau = 0.067 \pm 0.016$ PlanckTT+lensing+BAO (no P)
- ▶ Planck HFI low- ℓ polarization : $\tau = 0.053_{-0.016}^{+0.014}$ (E only)
 $\tau = 0.058 \pm 0.012$ (with T data included)
- ▶ The future.....limited by cosmic variance ($\Delta\tau \approx 0.006$, i.e., $\approx 10\%$)

SEARCHING FOR B MODES

E and B Mode Polarization



E mode

B mode

$$\mathbf{Y}_{\ell m,ab}^{(E)} = \sqrt{\frac{2}{(\ell-1)\ell(\ell+1)(\ell+2)}} \left[\nabla_a \nabla_b - \frac{1}{2} \delta_{ab} \nabla^2 \right] Y_{\ell m}(\hat{\Omega})$$

$$\mathbf{Y}_{\ell m,ab}^{(B)} = \sqrt{\frac{2}{(\ell-1)\ell(\ell+1)(\ell+2)}} \frac{1}{2} \left[\epsilon_{ac} \nabla_c \nabla_b + \nabla_a \epsilon_{bc} \nabla_c \right] Y_{\ell m}(\hat{\Omega})$$

Projection of « scalars, » « vectors » and « tensors » onto the celestial sphere

Under projection onto the celestial sphere :

$$(\text{scalar})_3 \rightarrow (\text{scalar})_2,$$

$$(\text{vector})_3 \rightarrow (\text{scalar})_2 + (\text{vector})_2,$$

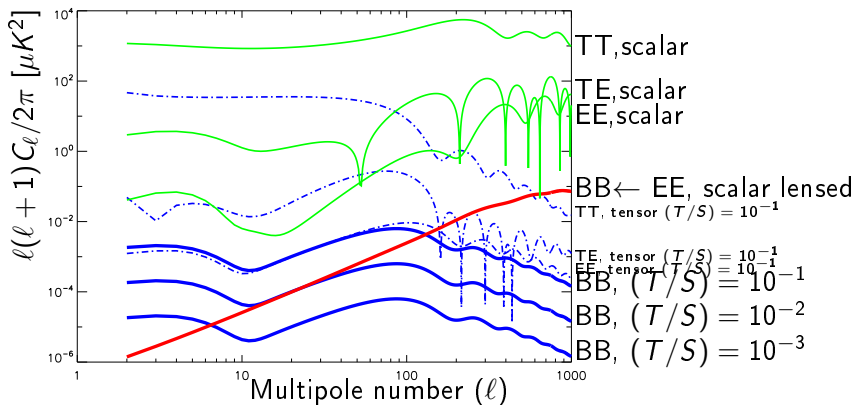
$$(\text{tensor})_3 \rightarrow (\text{scalar})_2 + (\text{vector})_2.$$

There is no $(\text{tensor})_2$ component. The E mode polarization is scalar; the B mode is vector.

It follows that at linear order the scalar modes cannot generate any B mode polarization.

Note crucial role of linearity assumption.

Inflationary Prediction for Scalar & Tensor Anisotropies



Lensing of the E mode into the B mode — $(E^{scalar} + \Phi \rightarrow B^{scalar})$

(Flat sky approximation : $(\ell m) \rightarrow \ell$, $\theta, \ell \in \mathcal{R}^2.$)

$$\delta\theta = (\nabla\Phi), \quad \delta T(\theta) = (\nabla\Phi) \cdot (\nabla T).$$

$$\delta T(\ell_F) = \int \frac{d^2\ell_L}{(2\pi)^2} (-\ell_L) \cdot (\ell_F - \ell_L) \Phi(\ell_L) T(\ell_F - \ell_L).$$

$$\langle T(\ell) T(\ell') \rangle = (2\pi)^2 \delta^2(\ell + \ell') C^{TT}(\ell)$$

$$C^{TT}(\ell_F) = \int \frac{d^2\ell_L}{(2\pi)^2} [\ell_L \cdot (\ell_F - \ell_L)]^2 C^{\Phi\Phi}(\ell_L) C^{TT}(\ell_I = |\ell_F - \ell_L|)$$

$$C^{BB}(\ell_B) = \int \frac{d^2\ell_L}{(2\pi)^2} [\ell_L \cdot (\ell_F - \ell_L)]^2 \sin^2[2\Theta(\ell_B, \ell_E)] C^{\Phi\Phi}(\ell_L) C^{EE}(\ell_E = |\ell_B - \ell_L|)$$

Characterizing the B modes

- ▶ What is n_T ? How accurately can we measure it? How important is it to fix n_T ?
- ▶ Detecting primordial B modes in more than one window?
- ▶ Are the B modes Gaussian? If not, what are the theoretically motivated templates for B mode non-Gaussianity?
- ▶ What about other non-standard mechanisms for generating B modes? Cosmic strings and other topological defects? Vector modes?
- ▶ If observed, do the primordial B modes violate parity symmetry? Chiral B modes.

On the theoretical front, the possibility of searching for non-Gaussianity was once considered outside the mainstream : non-standard models such as those with isocurvature modes or other quantum fields to break statistical isotropy were considered heresies. But with the prospect of the forthcoming Planck data, exploring ‘non-standard’ models became a very active and exciting area of theoretical investigation.

This story is likely to repeat itself for B modes.



3)/4) Origin of gravitational waves

M. Shiraishi, C. Hikage, T. Namikawa, R. Namba, MH, arXiv: [I 606.06082](#)

Vacuum fluctuation

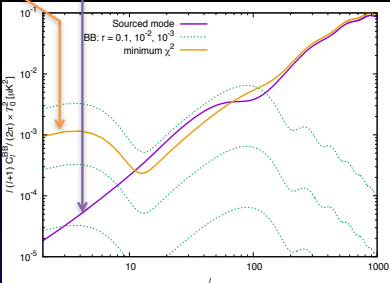
vs.

Source fields

Observation of $l < 10$ is required to distinguish between two.

At LiteBIRD, this can be done easily.

Moreover, B-mode bi-spectrum (“BBB”) is also used to detect source-field-originating non-Gaussianity at $>3\sigma$



“Pseudoscalar model” from Namba, Peloso, Shiraishi, Sorbo, Unal, arXiv: [I 509.07521](#) as an “evil example model”; indistinguishable w/ BB for ell > 10 alone.

Breaking news 22 March 2014

The Economist

World politics Business & finance Economics Science & technology Culture

Astrophysics

BICEP flexes its muscles

A telescope at the South Pole has made the biggest cosmological discovery so far this century

Mar 22nd 2014 | From the print edition

Timekeeper

Like 204

Tweet 39

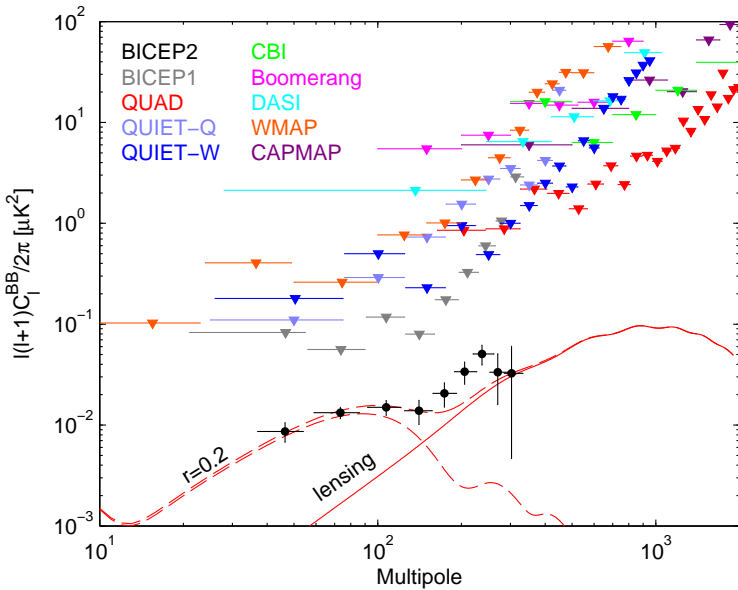


Keith Vanderlinde/National Science Foundation

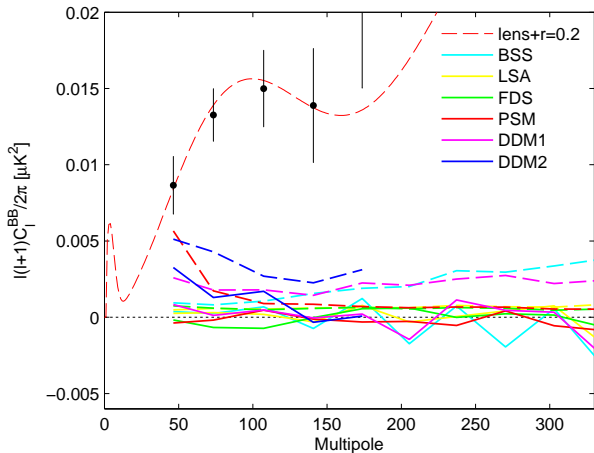
ONE useful feature of a scientific theory is that it makes testable predictions. Such predictions, though, do not have to be testable straight away. Physics is replete with prophecies that could be confirmed or denied only decades later, once the technology to examine them had caught up. The Higgs boson, for example, was 50 years in the confirming.

BICEP2 summary plot :

"Smoking gun" of gravitational waves from inflation ?



Why they said that dust cannot explain observed signal?





Stanford Professor Andrei Linde celebrates physics breakthrough



Stanford



S'abonner

369 701

2 827 303

22 843

461



J'aime



Dé



Download ▾

À propos de

Partager

Ajouter à

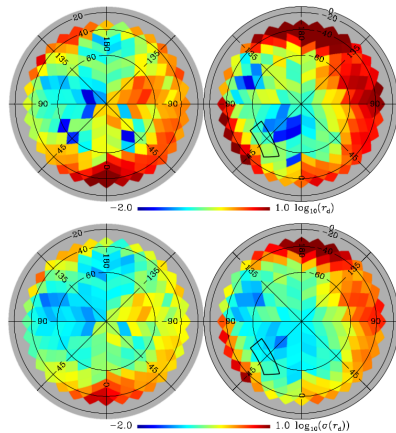


Ajoutée le 17 mars 2014

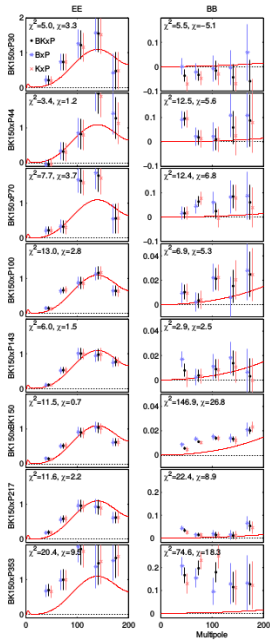
Assistant Professor Chao-Lin Kuo surprises Professor Andrei Linde with evidence that supports cosmic inflation theory. The discovery, made by Kuo and his colleagues at the BICEP2 experiment, represents the first images of gravitational waves, or ripples in space-time. These waves have been described as the "first

Disc

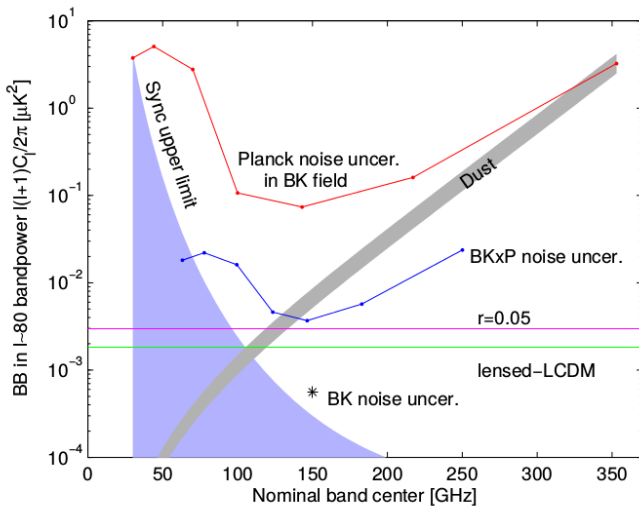
Planck Collaboration: Dust polarization at high latitudes



From Planck Collaboration : Dust polarization at high latitudes
(astro-ph/1409.5738)
Top : polarized dust as equivalent r .
Bottom : error in dust pol. measurement.



$r < 0.12$ at 95 % from B modes



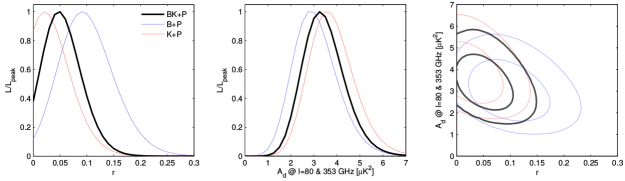


FIG. 6. Likelihood results from a basic lensed- Λ CDM+ r +dust model, fitting BB auto- and cross-spectra taken between maps at 150 GHz, 217, and 353 GHz. The 217 and 353 GHz maps come from *Planck*. The primary results (heavy black) use the 150 GHz combined maps from BICEP2/*Keck*. Alternate curves (light blue and red) show how the results vary when the BICEP2 and *Keck Array* only maps are used. In all cases a Gaussian prior is placed on the dust frequency spectrum parameter $\beta_d = 1.59 \pm 0.11$. In the right panel the two dimensional contours enclose 68% and 95% of the total likelihood.

$r < 0.12$ at 95 % from B modes

(now improved to $r < 0.07$) [Phys. Rev. Lett. 116, 031302, 2016]

LiteBIRD

A focused mission for discovering B modes from inflation



LiteBIRD

Lite (Light) Satellite for the studies of B-mode polarization and Inflation from cosmic background Radiation Detection (<http://litebird.jp/>)

LiteBIRD is a next generation scientific satellite aiming to measure polarization of Cosmic Microwave Background (CMB) at unprecedented sensitivity.

Mission Requirements:

- Measurement of B-mode polarization spectrum of large angular scale (by three-year observation of all sky).
- Measurement of the tensor-to-scaler ratio r , that represents primordial gravitational waves, at precision $\sigma_r < 0.001$ (w/o subtracting the gravitational lensing effect.)

The LiteBIRD Collaboration

M. Hazumi^{19,22,30,50}, P.A.R. Ade⁴⁸, Y. Akiba^{19,50}, D. Alonso⁴², K. Arnold¹⁶, J. Aumont²⁰, C. Baccigalupi²⁵, D. Barron⁴⁹, S. Basak^{11,25}, S. Beckman¹⁵, J. Borrill^{6,49}, F. Boulaenger²⁰, M. Bucher³, E. Calabrese⁴⁸, Y. Chihone^{15,30}, S. Cho¹³, A. Cukierman¹⁵, D.W. Curtiss⁴⁹, T. de Haan⁴⁴, M. Dobbs⁴³, A. Dominjon³⁵, T. Dotani²², L. Duband¹⁸, A. Ducout³⁰, J. Dunkley^{10,42}, J.M. Duval¹⁸, T. Ellefot¹⁶, H.K. Eriksen²⁴, J. Errard³, J. Fischer⁴⁹, T. Fujino⁵⁴, T. Funaki¹², U. Fuskeland²⁴, K. Ganga³, N. Goeckner-Wald¹⁵, J. Grain²⁰, N.W. Halverson^{4,9,17}, T. Hamada^{2,19}, T. Hasebe²², M. Hasegawa^{19,50}, K. Hattori³⁷, M. Hattori², L. Hayes⁴⁹, N. Hiedebara¹², C.A. Hill^{15,44}, G. Hilton³⁹, J. Hubmayr³⁹, K. Ichiki³², T. Iida³⁰, H. Imada²², M. Inoue⁴⁰, Y. Inoue^{19,21}, K.D. Irwin^{13,29}, H. Ishino¹², O. Jeong¹⁵, H. Kanai⁵⁴, D. Kaneko³⁰, S. Kashima³⁵, N. Katayama³⁰, T. Kawasaki³¹, S.A. Kernasovskiy¹³, R. Keskitalo^{6,49}, A. Kibayashi¹², Y. Kida¹², K. Kimura⁴⁰, T. Kisner^{6,49}, K. Kohri¹⁹, E. Komatsu³⁴, K. Komatsu¹², C.L. Kuo^{13,29}, N.A. Kurinsky^{13,29}, A. Kusaka^{14,44}, A. Lazarian⁵³, A.T. Lee^{15,44,45}, D. Li¹³, E. Linder^{44,49}, B. Maffei²⁰, A. Mangilli²⁰, M. Maki¹⁹, T. Matsumura³⁰, S. Matsuzura²⁷, D. Meilhan⁴⁹, S. Mima⁴⁶, Y. Minami¹⁹, K. Mitsuda²², L. Montier⁵, M. Nagai³⁵, T. Nagasaki¹⁹, R. Nagata¹⁹, M. Nakajima⁴⁰, S. Nakamura⁵⁴, T. Namikawa¹³, M. Naruse⁴⁷, H. Nishino¹⁹, T. Nitta⁵², T. Noguchi³⁵, H. Ogawa⁴⁰, S. Oguri⁴⁶, N. Okada²³, A. Okamoto²³, T. Okamura¹⁹, C. Otani⁴⁶, G. Patanchon³, G. Pisano⁴⁸, G. Rebeiz¹⁶, M. Remazeilles⁵¹, P.L. Richards¹⁵, S. Sakai²², Y. Sakurai³⁰, Y. Sato²³, N. Satoh¹⁹, M. Sawada¹, Y. Segawa^{19,50}, Y. Sekimoto^{8,22,50}, U. Seljak¹⁵, B.D. Sherwin^{7,28,44}, T. Shimizu⁸, K. Shinozaki²³, R. Stompor³, H. Sugai³⁰, H. Sugita²³, A. Suzuki^{15,45}, J. Suzuki¹⁹, O. Tajima^{19,50}, S. Takada³⁶, R. Takaku⁵⁴, S. Takakura^{19,41}, S. Takatori^{19,50}, D. Tanabe^{19,50}, E. Taylor⁴⁹, K.L. Thompson^{13,29}, B. Thorne^{30,42}, T. Tomaru¹⁹, T. Tomida²², N. Tomita¹, M. Tristram³³, C. Tucker¹⁶, P. Turin⁴⁹, M. Tsujimoto²², S. Uozumi¹², S. Utsunomiya³⁰, Y. Uzawa³⁸, F. Vansyngel²⁰, I.K. Wehus²⁴, B. Westbrook¹⁵, M. Willer⁴⁹, N. Whitehorn¹⁵, Y. Yamada¹², R. Yamamoto²², N. Yamasaki²², T. Yamashita⁵⁴, M. Yoshida¹⁹

¹Aoyama Gakuin University, Japan; ²Tohoku University, Japan; ³APC, France; ⁴University of Colorado, Boulder, USA; ⁵CNRS, IRAP, Toulouse, France; ⁶Lawrence Berkeley National Laboratory, Berkeley, USA; ⁷DAMTP, University of Cambridge, UK; ⁸The University of Tokyo, Japan; ⁹University of Colorado, Boulder, USA ¹⁰Princeton University, USA; ¹¹Amrita University, Kerala, India; ¹²Okayama University, Japan; ¹³Stanford University, USA; ¹⁴University of Tokyo, Japan; ¹⁵University of California, Berkeley, USA; ¹⁶University of California, San Diego, USA; ¹⁷University of Colorado, Boulder, USA; ¹⁸CEA, Grenoble, France; ¹⁹KEK, Tsukuba, Japan; ²⁰IAS, Orsay, France; ²¹Academia Sinica, Taiwan; ²²ISAS, JAXA, Japan; ²³JAXA, Tsukuba, Japan; ²⁴University of Oslo, Norway; ²⁵SISSA, Trieste, Italy; ²⁷Kansei Gakuin University, Japan; ²⁸Kavli Institute for Cosmology Cambridge, UK; ²⁹KIPAC, SLAC, USA; ³⁰Kavli IPMU, Japan; ³¹Kitazato University, Japan; ³²Nagoya University, Japan; ³³LAL, Univ. Paris-Sud, France ³⁴Max-Planck-Institut für Astrophysik, Garching, Germany; ³⁵NAOJ, Japan; ³⁶NIFS, Japan; ³⁷AIST, Japan; ³⁸NICT, Japan; ³⁹NIST, Boulder, Colorado, USA; ⁴⁰Osaka Prefecture University, Japan; ⁴¹Osaka University, Japan; ⁴²Oxford Astrophysics, United Kingdom; ⁴³McGill University, Montreal, Canada; ⁴⁴Lawrence Berkeley National Laboratory, USA; ⁴⁵Radio Astronomy Laboratory, Berkeley, USA; ⁴⁶RIKEN, Japan; ⁴⁷Saitama University, Japan; ⁴⁸Cardiff University, United Kingdom; ⁴⁹Space Sciences Laboratory, Berkeley, USA; ⁵⁰SOKENDAI, Japan; ⁵¹University of Manchester, United Kingdom; ⁵²University of Tsukuba, Japan; ⁵³University of Wisconsin-Madison, USA; ⁵⁴Yokohama National University, Japan

LiteBIRD-Japan/US/Europe

LiteBIRD :

- ▶ Led by Japanese Space Agency (JAXA) - Masashi Hazumi (PI)
- ▶ Large-class mission — 300 M USD cost cap
- ▶ Currently finishing Phase A1 study (Concept Development)
- ▶ Definitive selection to take place toward end of 2018
- ▶ Launch date envisaged for 2025-27
- ▶ Japan to take charge of launch, service module, low-frequency telescope, most of cooling chain

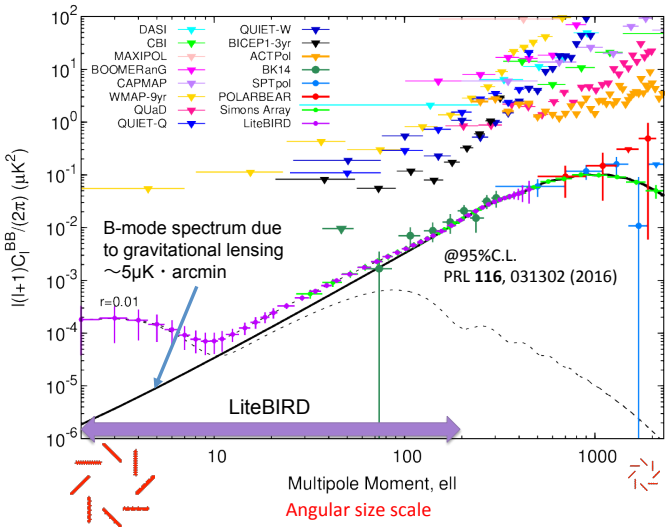
US Mission of Opportunity Participation :

- ▶ 65 M USD cost cap NASA explorer programme.
- ▶ Adrian Lee, UC Berkely, PI
- ▶ US Phase A study completed. Extra funds given for additional technology development
- ▶ To provide detectors and cold electronics

European Mission of Opportunity Participation :

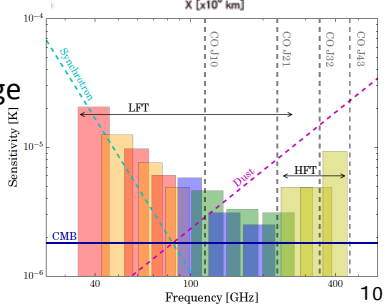
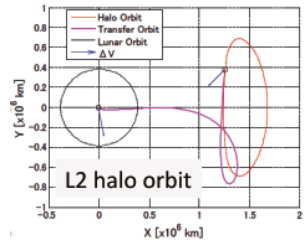
- ▶ In the process of being organized.
- ▶ Interest from France, Italy, UK, Germany, Spain, ...
- ▶ Possibility of up 50M euro ESA participation as well as national contributions.
- ▶ LiteBIRD-Europe meetings held in Cardiff, Paris and Torino (upcoming)

LiteBIRD Measurement Precision (at $r=0.01$)

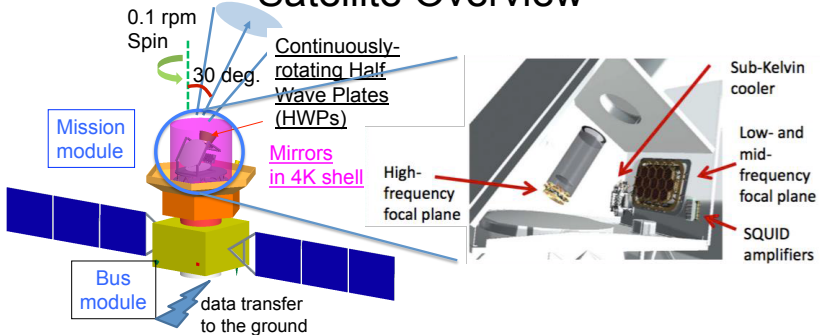


Mission specification

- Operation at Lagrange-point 2
- Full-sky scan
- Optimized for large-angle polarization structure from primordial B-mode signal
- High detector sensitivity:
3 μK arcmin with margin
- Wide frequency band coverage
(40-400 GHz, 15 bands)
- Launch around 2025-2027
- 3 years operation

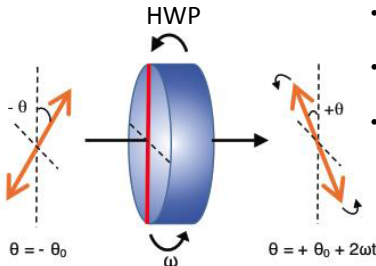


Satellite Overview



- Satellite consists of two modules : low-temp. mission part and normal-temp bus part.
- Rotating HWP modulates incoming signal.
- Two complementary optics : LFT and HFT to cover wide freq. bands.
- Optics are kept under 4K by JT/ST and ADR cryogenics.
- Superconducting detectors (TES) are arranged on focal planes.

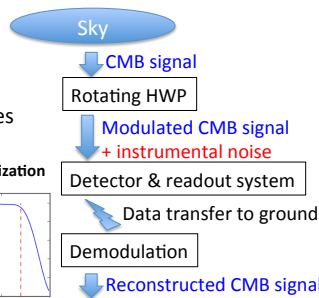
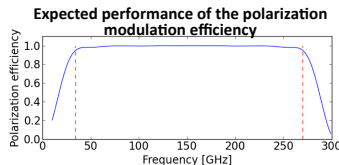
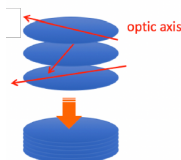
Rotating Half Wave Plate



- HWP changes direction of polarization with respect to a fixed axis.
- Modulation of CMB signal by rotating HWP reduces 1/f noise.
- Other instrumental systematics can be greatly reduced by rotating HWP.

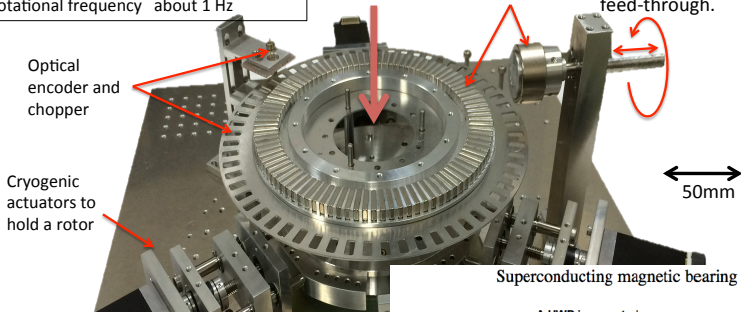
JPS_Sep2016_23aSR-9, Sakurai et al.

- Stacking several layers of rotating HWP makes freq. bandwidth wider.

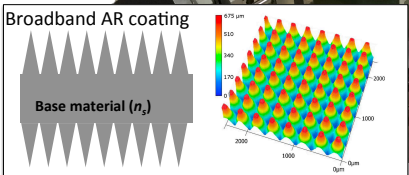


HWP Small diameter prototype rotational mechanism

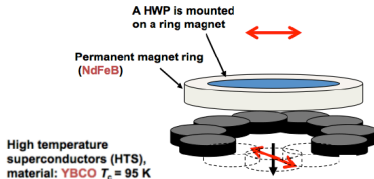
Aperture (a half-wave plate diameter)
Φ50mm
Operation temperature <10 K
Rotational frequency about 1 Hz



The shaft is coupled to a motor mounted outside of the cryostat via linear/rotational feed-through.

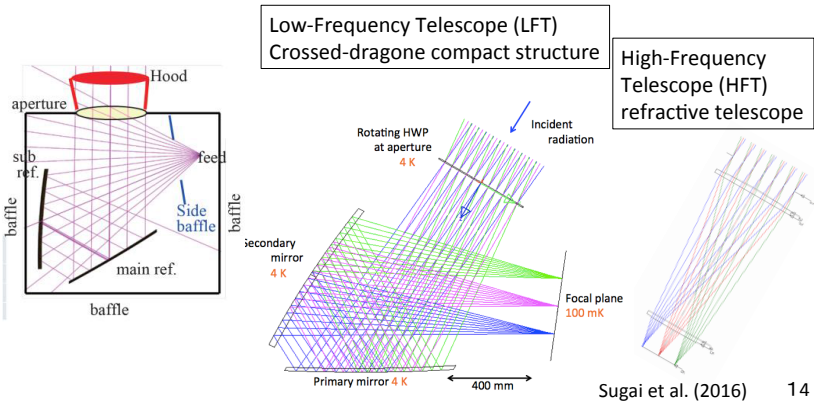


Superconducting magnetic bearing (SMB)

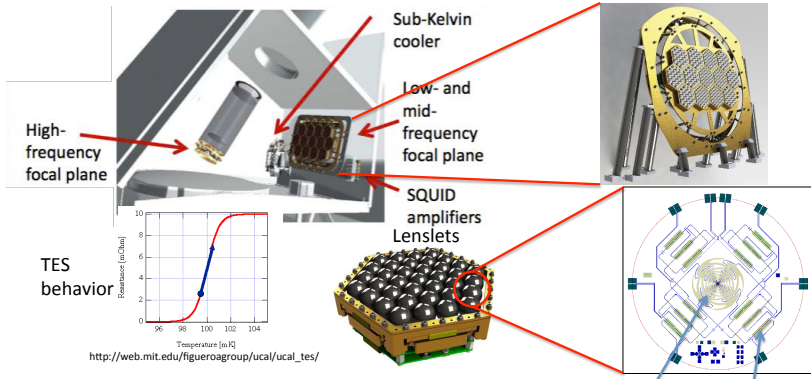


Optical System

- Beam size : < 1 deg. at all the observing band
- FOV: 10 x 20 degs.
- Aperture Size: 40cm
- Covered by 4K shell
- Cold Baffle and Mirrors



Focal Plane Detectors



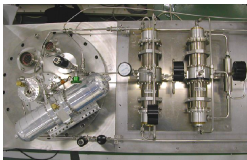
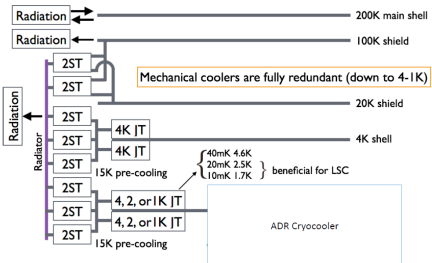
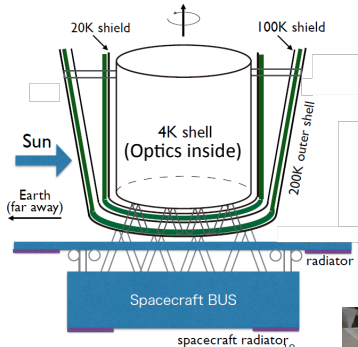
- Focal planes consist of arrays of detectors
- Each detector array covers certain freq. band
- Behind lenslet antenna and bolometers are arranged
- Bolometers (Transition Edge Sensors) are cooled to ~100mK to detect signals
- Signal readout from Bolometer by SQUID

Sinus antenna

Bolometers
(TES)

Cryogenic system

Cryogenic system above 2 K



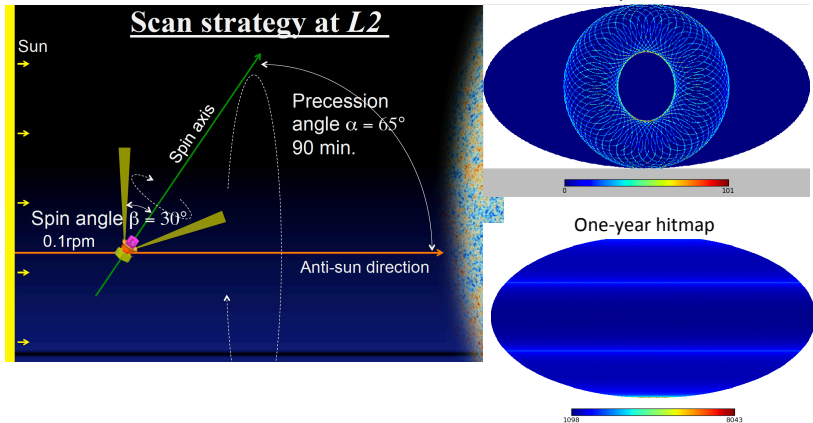
JT and ST coolers



ADR cryocooler

- Cryogenic system consists of JT/ST and ADR coolers.
- Covering optics in 4K shell is important to reduce thermal noise.

All Sky Scan Strategy



- Precession + spin angle < 95 deg. for full anti-sun direction scan
- Satellite scans all sky at L2 combining “precession” and “spin” motion

Basic reference :

 Cornell University
Library

arXiv.org > astro-ph > arXiv:1501.04288

Astrophysics > Cosmology and Nongalactic Astrophysics

Physics of the cosmic microwave background anisotropy

Martin Bucher (Laboratoire APC, Université Paris 7/CNRS, Paris, France and School of Mathematics, Statistics and Computer Science, University of KwaZulu-Natal, Durban, South Africa)

(Submitted on 18 Jan 2015)

Observations of the cosmic microwave background (CMB), especially of its frequency spectrum and its anisotropies, both in temperature and in polarization, have played a key role in the development of modern cosmology and our understanding of the very early universe. We review the underlying physics of the CMB and how the primordial temperature and polarization anisotropies were imprinted. Possibilities for distinguishing competing cosmological models are emphasized. The current status of CMB experiments and experimental techniques with an emphasis toward future observations, particularly in polarization, is reviewed. The physics of foreground emissions, especially of polarized dust, is discussed in detail, since this area is likely to become crucial for measurements of the B modes of the CMB polarization at ever greater sensitivity.

Comments: 105 pages, 26 figures

Subjects: Cosmology and Nongalactic Astrophysics (astro-ph.CO)

DOI: 10.1142/S0216271815300049

Cite as: arXiv:1501.04288 [astro-ph.CO]

(or arXiv:1501.04288v1 [astro-ph.CO] for this version)